Advances in Applied Mathematics and Mechanics
Adv. Appl. Math. Mech., Vol. **14**, No. 1, pp. 218-247

DOI: 10.4208/aamm.OA-2020-0202
February 2022

Buckling Analysis of FG Porous Truncated Conical Shells Resting on Elastic Foundations in the Framework of the Shear Deformation Theory

Le Kha Hoa[1], Bui Gia Phi[2], Do Quang Chan[3,4,*] and Dang Van Hieu[5]

[1] *Military Academy of Logistics, Hanoi, Vietnam*
[2] *Department of Technical Fundamental, University of Transport Technology, 54 Trieu Khuc, 9 Thanh Xuan, Hanoi, Vietnam*
[3] *Department of Mechanical Engineering and Mechatronics, PHENIKAA University, Hanoi 12116, Vietnam*
[4] *PHENIKAA Research and Technology Institute (PRATI), A&A Green Phoenix Group JSC, No. 167 Hoang Ngan, Trung Hoa, Cau Giay, Hanoi 11313, Vietnam*
[5] *Thainguyen University of Technology, Thainguyen, Vietnam*

Received 4 July 2020; Accepted (in revised version) 14 October 2020

Abstract. In this article, an analytical method is proposed to analyze of the linear buckling behavior of the FG porous truncated conical shells subjected to a uniform axial compressive load and resting on the Pasternak elastic foundation. The material properties including Young's modulus, shear modulus and density are assumed to vary in the thickness direction. Three types of FG porous distributions including symmetric porosity distribution, non-symmetric porosity and uniform porosity distribution are considered. The governing equations of the FG porous truncated conical shells are obtained by using the first-order shear deformation theory (FSDT). With the help of the Galerkin method, the expressions for critical buckling loads are obtained in closed forms. The reliability of the obtained results is verified by comparing the present solutions with the published solutions. Finally, the numerical results show the effects of shell characteristics, porosity distribution, porosity coefficient, and elastic foundation on the critical buckling load.

AMS subject classifications: 74K25, 74G60

Key words: Buckling, truncated conical shells, first order shear deformation theory, porous materials, elastic foundations.

*Corresponding author.
Emails: lekhahoa@gmail.com (L. Hoa), phibg@utt.edu.vn (B. Phi), chan.doquang@phenikaa-uni.edu.vn (D. Chan), hieudv@tnut.edu.vn (D. Hieu)

1 Introduction

Structures fabricated from functionally graded materials (FGMs) are usually found in kinds of engineering applications, such as pressure vessels, nuclear reactors, spacecraft, submarines, jet nozzles and other such civil, mechanical, aerospace engineering structures and chemical. The investigations on the stability, buckling, and free vibration analysis of FGM evaluated by different authors worldwide in the past few decades. Javaheri and Eslami [1] studied thermal buckling behavior of functionally graded (FG) plates by using the higher-order shear deformation plate theory. Based on Love–Kirchhoff hypothesis and Sander's non-linear strain-displacement relation, Najafizadeh and Eslami [2] investigated the buckling analysis of FG circular plate under a radial load. Using FSDT, Liew et al. [3] analyzed thermal buckling and post-buckling of thick laminated rectangular FG plates. Based on the classical shell theory with von Karman–Donnell-type of kinematic nonlinearity, Shen [4, 5] studied the thermal post-buckling behavior of FG cylindrical shell subjected to compressive axial loads and external pressure. In [6], Shen investigated the thermal post-buckling response of a shear deformable FG cylindrical shell embedded in an elastic medium. Using the Ritz energy method and the nonlinear strain–displacement relations of large deformation, Huang and Han [7] studied the nonlinear buckling and post-buckling responses of FG cylindrical shells under axially compressive load. Duc [8] investigated the nonlinear thermal dynamic behavior of imperfect FG cylindrical shells reinforced by outside stiffeners and surrounded on elastic foundations using the third-order shear deformation shells theory in thermal environment. The nonlinear response of thick sigmoid FG cylinder with temperature-independent material property surrounded on elastic layers and subjected to mechanical and thermal loads was investigated by Duc et al. [9]. Using both of the first-order shear deformation theory and stress function with full-motion equations, Duc and Thang [10] studied the nonlinear dynamic response and vibration of imperfect ES-FGM cylinder subjected to mechanical and damping loads and surrounded on elastic layers. Dung and Hoa [11] investigated the thermal nonlinear buckling and post-buckling of FG stiffened cylindrical shells embedded in a Pasternak medium and subjected to torsional load. Based on the Donnell theory of shells and the von-Karman type of geometrical nonlinearity, Sabzikar Boroujerdy et al. [12] investigated thermal buckling behavior of cylindrical shells resting on the Pasternak foundation with regard to temperature dependency of the constituents. Using the generalized differential quadrature method and FSDT, Tornabene et al. [13] investigated the static and dynamic of laminated doubly-curved shells and panels of revolution resting on the elastic foundation. Duc and Quan [14] investigated the nonlinear dynamic response and vibration of imperfect ES-FGM double curved thin shallow shells on elastic foundation. In [15], based on Reddy's higher-order shear deformation shell theory, Duc and Quan analyzed the nonlinear static and dynamic stability of imperfect eccentrically stiffened FG double curved shallow shell on elastic foundations in thermal environments. Sofiyev and Aksogan [16] studied the buckling of a truncated conical shell under a uniform external pressure. The shell is asummed to have a meridional thickness described

by an arbitrary function. Based on the first-order shell theory and the Sanders nonlinear kinematics equations, Naj et al. [17] investigated thermal and mechanical instability of FG truncated conical shells. Using the large deformation theory with von Karman–Donnell-type of kinematic non-linearity, Sofiyev [18] studied the non-linear buckling response of FG truncated conical shells subject to a uniform axial compressive load. Based on the classical shell theory and smeared stiffeners technique, Dung et al. [19] presented the mechanical buckling behavior of an ES-FG truncated conical shells subjected to axial compressive load and external uniform pressure. Torabi et al. [20] investigated the linear buckling analysis of a FG conical shell integrated with piezoelectric layers subjected to both thermal and electrical loads. Based on the classical shell theory taking into account geometrical nonlinearity, Duc and Cong [21] studied the thermal stability of an eccentrically stiffened FG truncated conical shells in the thermal environment and surrounded on the Pasternak type elastic foundations. Based on the Donnell shell theory assumptions consistent with FSDT, the linear buckling problem of nanocomposite conical shells reinforced with single-walled carbon nanotubes subjected to lateral pressure was studied by Jam and Kiani [22]. Sofiyev [23] studied the non-linear free vibration of FG orthotropic cylindrical shells taking into account the shear stresses based on FSDT and von Karman-type strain displacement relationships. An analytical method was ultilized by Dung and Chan [24] to analyze the mechanical buckling of FG truncated conical shells subjected to axial compressive load and external uniform pressure. Duc et al. [25] analyzed the mechanical and thermal buckling behaviors of FG sandwich truncated conical shells subjected to both thermal and axial compressive loads.

Porous materials are a relatively new class of engineering materials that can serve functional and structural purposes. They widely exist around us and play a role in many aspects of our daily lives. These lightweight materials not only have the typical characteristics of metals (weldability, electrical conductivity, and ductility), but also possess other useful characteristics, such as low density, high specific surface area, low thermal conductivity, great penetrability, energy management, mechanical damping, vibration suppression, sound absorption, noise attenuation, and electromagnetic shielding. Therefore, these materials have increasing applications and have emerged as a focus of great attention in the material field. Buckling and vibration problems of the porous structures have been developed by many authors. Zhang et al. [26] studied numerically dynamic responses of clamped-clamped sandwich beams made of aluminum face sheets and close-celled aluminum foam cores. There are three types of foam core considered in this work including homogeneous core, low-high gradient-density core and high-low gradient-density core. Chen et al. [27] investigated the buckling and static bending of shear deformable FG porous Timoshenko beams. Expressions of the critical buckling loads and transverse bending deflections are obtained by employing Ritz method. Chen et al. [28] also studied the nonlinear free vibration response of the shear deformable sandwich porous Timoshenko beam with a FG porous core. The beams are composed of two face layers and a FG porous core which includes the internal pores following different porosity distributions. Fouda et al. [29] investigated the effect of poros-

ity on the mechanical behaviors of a FG Euler-Bernoulli beam by using the finite element method. Wattanasakulpong et al. [30] carried out vibration analysis of FG porous beams using TSDT. The beams have the. Both uniform and non-uniform porosity distributions across thickness direction of beams are considered in this paper. An analytical method was employed by Ziane et al. to predict the thermal buckling of simply supported and clamped-clamped FG box beams [31]. The expression of the critical moment for simply supported beams under thermo-mechanical loads is obtained by using Galerkin's method. Magneto-electro-elastic buckling and vibration behaviors of a sandwich Timoshenko beam with a porous core and polyvinylidene fluoride matrix were investigated by Bamdad et al. [32]. Based on the nonlocal strain gradient theory, She et al. [33] analyzed the nonlinear bending and vibration responses of porous tubes. She et al. [34] studied the nonlinear bending behavior of FG porous curved nanotubes. Jabbari et al. [35] studied buckling behavior of a porous rectangular plate in undrained conditions. Distributing of the pores including the nonlinear nonsymmetric, nonlinear symmetric, and monotonous distributions are considered in this paper. Jabbari et al. [36] presented the buckling analysis of thermal loaded porous circular plate. Khorshidvand et al. [37] presented the buckling analysis of a porous circular plate bounded with piezoelectric sensor-actuator patches. Based on higher order shear deformation theory, Mojahedin et al. [38] studied the buckling bihavior of a saturated porous circular plate. Arani et al. [39] studied the dynamic response of a porous rectangular plate resting on a Pasternak layer based on Reddy's third-order shear deformation theory. The four-variable shear deformation refined plate theory is proposed by Ebrahimi et al. [40] to analyze the free vibration response of porous magneto-electro-elastic FG plates. Using a semi-analytical method, Zhao et al. [41] provided parameterization study for vibration behavior of FG porous doubly-curved panels and shells of revolution. Three types of uniform or non-uniform porosity distributions were considered in this work. Based on the FSDT, Duc et al. [42] studied the nonlinear dynamic response of FG porous plates under thermal and mechanical loadings supported by elastic foundation. Both evenly distributed porosities and unevenly distributed porosities assumed as effective properties of FG plates were considered. Wang [43] investigated electro-mechanical vibrations of FG piezoelectric material plates carrying porosities in the translation state by employing Galerkin's method and the harmonic balance method. Coskun et al. [44] studied static bending, buckling and free vibration of FG porous micro-plates using a third order plate theory. Three different porosity distributions were considered and the effects of porosity variations were examined. In the framework of isogeometric analysis, Xue et al. [45] studied the free vibration of porous square plate, circular plate, and rectangle plate with a central circular hole. In this study, the porosity distributions along both the thickness direction and in-plane direction were considered. Nam et al. [46] presented nonlinear buckling and post-buckling behavior of stiffened porous functionally graded plate rested on Pasternak's elastic foundation under mechanical load in thermal environment by an analytical approach.

A sinusoidal shear deformation theory and the Rayleigh–Ritz method were employed by Wang and Wu [47] to investigate the free vibration of a FG porous cylindrical shell

under different sets of immovable boundary conditions. Li et al. [48] provided a new semi-analytical method to analyze the free vibration of FG porous cylindrical shells with arbitrary boundary restraints. Nam et al. [49] investigated the thermal nonlinear buckling and post-buckling of FG porous circular cylindrical shells reinforced by orthogonal stiffeners resting on Pasternak layers and subjected to torsional load. Based on FSDT, Pang et al. [50] investigated the vibration behavior of the FG spherical shell with general boundary conditions. Rahmani et al. [51] studied vibration behavior of the truncated conical sandwich shells including temperature dependent porous FG face sheets and temperature dependent homogeneous core in various thermal conditions. The nonlinear buckling and post-buckling characteristics of the porous ES-FG sandwich truncated conical shells under axial compressive loads were investigated by Thai et al. [52].

The above-introduced works about FG porous structures show that they only focus on beam and plate structures, and investigations involving the application of FG porous shells are still limited in number. Nowadays, in engineering practices, the shell structures such as cylindrical shells, toroidal shells and conical shells are widely used in all kinds of fields in order to match the desired functionality and optimize the structures. Thus, it is of great importance to analyze buckling, dynamic response and vibration behavior of FG porous shells. However, to the best of the authors' knowledge, there is no previous work related to buckling analysis of FG porous truncated conical shells with different internal porosities.

The novelty of this paper is the first time using the analytical approach to investigate the buckling of FG porous truncated conical shells. The shells are assumed to rest on the Winkler–Pasternak elastic foundation and subject to a uniform axial compressive load. Distribution of the porous through the thickness of the structures may be uniform or non-uniform and three types of the porosity distributions that are symmetric porosity distribution, non-symmetric porosity distribution, and uniform porosity distribution are considered. Based on the first-order shear deformation theory, the governing equations, including the equilibrium and stability equations for FG porous truncated conical shells, are derived and solved by using the Galerkin's method. Expressions of the critical buckling loads of FG porous truncated conical shells with simply supported boundary condition are obtained in the closed-forms. Finally, the results are compared with the buckling loads of FG porous truncated conical shells obtained in the literature and the influences of porosity distribution, porosity coefficient, shell characteristics, and elastic foundation on the critical buckling loads of shells are considered in detail.

2 Kinematic relations and the constitutive laws of FG porous truncated conical shells

2.1 Functionally graded porous truncated conical shell

A truncated conical shell is considered. The geometry of the shell is shown in Fig. 1(a), where L is the length, h is thickness, β is semi-vertex angle of the truncated conical shell, and R inndicate the radii of the truncated conical shell at its small end. Also, x_0 indicates the distance from the vertex to the small base of the shell.

Moreover, assuming that the truncated conical shell is made of FG porous materials and distribution of the porous through the thickness of the shell is uniform or non-uniform and three three types of FG porous distributions [41], namely Type 1 (symmetric porosity distribution), Type 2 (non-symmetric porosity distribution) and Type 3 (uniform porosity distribution), as show in Fig. 2. The variation of Young's modulus $E(z)$, shear modulus $G(z)$ and density $\rho(z)$ through the thickness direction of the FG porous truncated conical shell are described by Eqs. (2.1)-(2.4) [35, 41, 48].

Type 1: symmetric porosity distribution

$$E(z)=E_{\max}\left[1-e_0\cos\left(\frac{\pi z}{h}\right)\right], \tag{2.1a}$$

$$G(z)=G_{\max}\left[1-e_0\cos\left(\frac{\pi z}{h}\right)\right], \tag{2.1b}$$

$$\rho(z)=\rho_{\max}\left[1-e_m\cos\left(\frac{\pi z}{h}\right)\right], \tag{2.1c}$$

Type 2: non-symmetric porosity distribution

$$E(z)=E_{\max}\left[1-e_0\cos\left(\frac{\pi z}{2h}+\frac{\pi}{4}\right)\right], \qquad G(z)=G_{\max}\left[1-e_0\cos\left(\frac{\pi z}{2h}+\frac{\pi}{4}\right)\right], \tag{2.2a}$$

$$\rho(z)=\rho_{\max}\left[1-e_m\cos\left(\frac{\pi z}{2h}+\frac{\pi}{4}\right)\right], \qquad E(z)=E_{\max}\left[1-e_0\sin\left(\frac{\pi z}{2h}+\frac{\pi}{4}\right)\right], \tag{2.2b}$$

$$G(z)=G_{\max}\left[1-e_0\sin\left(\frac{\pi z}{2h}+\frac{\pi}{4}\right)\right], \qquad \rho(z)=\rho_{\max}\left[1-e_m\sin\left(\frac{\pi z}{2h}+\frac{\pi}{4}\right)\right], \tag{2.2c}$$

Type 3: uniform porosity distribution

$$E(z)=E_{\max}(1-e_0\lambda), \quad G(z)=G_{\max}(1-e_0\lambda), \quad \rho(z)=\rho_{\max}\sqrt{1-e_m\lambda}, \tag{2.3}$$

where z is the coordinate in the thickness direction; e_0 is the porosity coefficient ($0\le e_0\le 1$) and can be obtained by

$$e_0=1-\frac{E_{\min}}{E_{\max}}=1-\frac{G_{\min}}{G_{\max}}, \quad e_m=1-\frac{\rho_{\min}}{\rho_{\max}}, \quad 0\le e_m\le 1.$$

$E_{\min}$, $G_{\min}$ and $\rho_{\min}$ are the minimum values of Young's modulus, shear modulus and mass density in the thickness direction of the truncated conical shells, respectively; while $E_{\max}$, $G_{\max}$ and $\rho_{\max}$ are the corresponding maximum values, respectively. When $e_0=e_m=0$, it indicates that the special case with no pore exists. And whereas $e_0=e_m=1$ cannot be achieved in this case because all material property values are reduced to zero. Based on

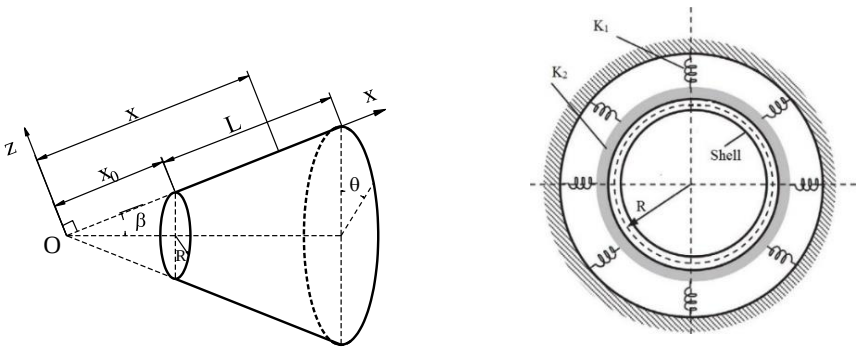

(a) Truncated cone model (b) Shell on elastic foundation

Figure 1: FG porous truncated cone embedded in a Pasternak elastic foundation.

the typical mechanical property of open-cell metal foam, the relationship between e_0 and e_m and the coefficient λ in uniform porosity distribution are defined as

$$e_m = 1-\sqrt{1-e_0}, \quad \lambda = \frac{1}{e_0} - \frac{1}{e_0}\left(\frac{2}{\pi}\sqrt{1-e_0}+\frac{2}{\pi}+1\right)^2. \tag{2.4}$$

The Poisson's ratio ν is assumed to be constant: $\nu = const$.

The FG porous truncated conical is assumed to be embedded in the Pasternak elastic foundation (Fig. 1(b)). The foundation interface pressure is expressed as [8,9,12,13]

$$q_f(x,\theta) = K_1 w - K_2\left(\frac{\partial^2 w}{\partial x^2}+\frac{1}{x}\frac{\partial w}{\partial x}+\frac{1}{x^2\sin^2\beta}\frac{\partial^2 w}{\partial \theta^2}\right), \tag{2.5}$$

in which w is the deflection of the conical shells, K_1 is the Winkler foundation modulus and K_2 is the shear layer foundation stiffness of the Pasternak model.

2.2 Fundamental relations

Using FSDT and the Timoshenko-Mindlin assumption, the displacements at a point are represented in displacement components u, v, w of a point in the middle surface in the direction x, θ and z, respectively [17,20,22,54,55]

$$u_x = u + z\phi_x, \quad u_\theta = v + z\phi_\theta, \quad u_z = w, \tag{2.6}$$

in which ϕ_x, ϕ_θ are the rotations of a transverse normal about the θ and x-axes, respectively.

The normal and shear strains across the shell thickness of an FG porous truncated conical shells at a distance z away from the middle surface are

$$\varepsilon_x = \varepsilon_{xm} + zk_x, \quad \varepsilon_\theta = \varepsilon_{\theta m} + zk_\theta, \quad \gamma_{x\theta} = \gamma_{x\theta m} + 2zk_{x\theta}, \quad \gamma_{xz} = \gamma_{xzm}, \quad \gamma_{\theta z} = \gamma_{\theta zm}, \tag{2.7}$$

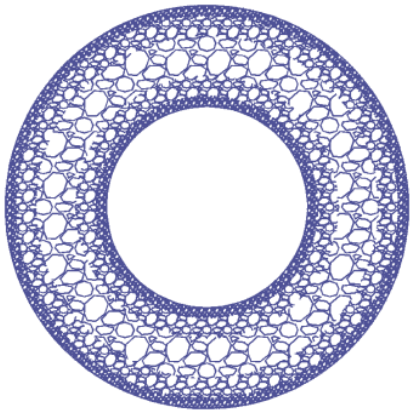

(a) Type 1: Symmetric porosity distribution

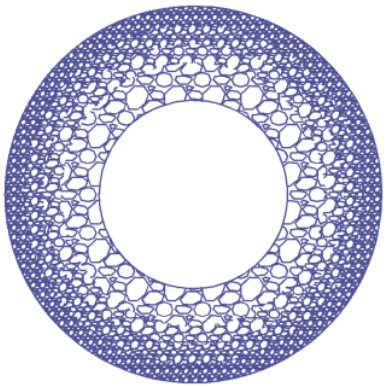

(b) Type 2a: Non-symmetric porosity distribution

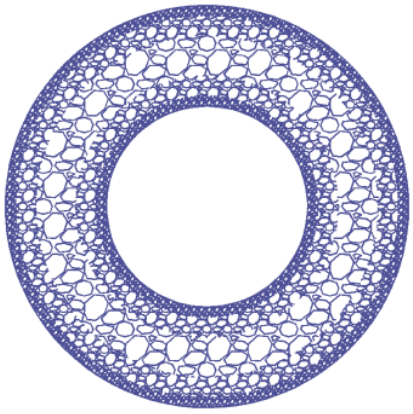

(c) Type 2b: Non-symmetric porosity distribution

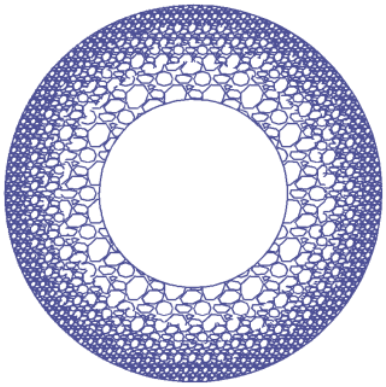

(d) Type 3: Uniform porosity distribution

Figure 2: Cross-section of a FG porous truncated cone with different porosity distributions.

where x and θ are the normal strains, $\gamma_{x\theta}$ is the shear strain, k_x and k_θ are the middle surface curvature changes and $k_{x\theta}$ is the middle surface twist. In Eq. (2.7) the subscript m refers to the middle surface of the shell.

The strains, curvature changes, and twist of the middle surface of an FG porous truncated conical shells are related to the displacement components as [17,20,54,55,57]

$$\varepsilon_{xm}=u_{,x}+\frac{1}{2}w_{,x}^2,\quad \varepsilon_{\theta m}=\frac{1}{x\sin\beta}v_{,\theta}+\frac{u}{x}+\frac{w}{x}\cot\beta+\frac{1}{2x^2\sin^2\beta}w_{,\theta}^2, \tag{2.8a}$$

$$\gamma_{x\theta m}=\frac{1}{x\sin\beta}u_{,\theta}-\frac{v}{x}+v_{,x}+\frac{1}{x\sin\beta}w_{,x}w_{,\theta},\quad \gamma_{xzm}=w_{,x}+\phi_x, \tag{2.8b}$$

$$\gamma_{\theta zm}=\frac{1}{x\sin\beta}w_{,\theta}+\phi_\theta,\quad k_x=\phi_{x,x}, \tag{2.8c}$$

$$k_\theta=\frac{1}{x\sin\beta}\phi_{\theta,\theta}+\frac{1}{x}\phi_x,\quad k_{x\theta}=\frac{1}{2}\left[\phi_{\theta,x}+\frac{1}{x\sin\beta}\phi_{x,\theta}-\frac{1}{x}\phi_\theta\right], \tag{2.8d}$$

where subscript $(,)$ indicates the partial differentiation.

The stress–strain relations for the FG porous truncated conical shells based on Hooke law are [17,20,57]

$$\sigma_x^{sh}=\frac{E_{sh}}{1-\nu^2}(\varepsilon_x+\nu\varepsilon_\theta),\quad \sigma_\theta^{sh}=\frac{E_{sh}}{1-\nu^2}(\varepsilon_\theta+\nu\varepsilon_x), \tag{2.9a}$$

$$\sigma_{x\theta}^{sh}=\frac{E_{sh}}{2(1+\nu)}\gamma_{x\theta},\quad \sigma_{xz}^{sh}=\frac{E_{sh}}{2(1+\nu)}\gamma_{xzm},\quad \sigma_{\theta z}^{sh}=\frac{E_{sh}}{2(1+\nu)}\gamma_{\theta zm}. \tag{2.9b}$$

The force and moment resultants are defined as [8,28]

$$N_i=\int_{-\frac{h}{2}}^{\frac{h}{2}}\sigma_i dz,\quad M_i=\int_{-\frac{h}{2}}^{\frac{h}{2}}z\sigma_i dz,\quad (i=x,\theta), \tag{2.10a}$$

$$N_{x\theta}=\int_{-\frac{h}{2}}^{\frac{h}{2}}\sigma_{x\theta}dz,\quad M_{x\theta}=\int_{-\frac{h}{2}}^{\frac{h}{2}}x\sigma_{x\theta}dz,\quad Q_x=\frac{5}{6}\int_{-\frac{h}{2}}^{\frac{h}{2}}\sigma_{xz}dz,\quad Q_\theta=\frac{5}{6}\int_{-\frac{h}{2}}^{\frac{h}{2}}\sigma_{\theta z}dz. \tag{2.10b}$$

Substituting Eqs. (2.6)-(2.9) into Eq. (2.10) yields, after integrating and rearrangements, the equations for force and moment resultants, and transverse force resultants as

$$N_x=A_{11}\varepsilon_{xm}+A_{12}\varepsilon_{\theta m}+B_{11}k_x+B_{12}k_\theta, \tag{2.11a}$$

$$N_\theta=A_{12}\varepsilon_{xm}+A_{22}\varepsilon_{\theta m}+B_{12}k_x+B_{22}k_\theta, \tag{2.11b}$$

$$N_{x\theta}=A_{66}\gamma_{x\theta m}+2B_{66}k_{x\theta}, \tag{2.11c}$$

and

$$M_x=B_{11}\varepsilon_{xm}+B_{12}\varepsilon_{\theta m}+D_{11}k_x+D_{12}k_\theta, \tag{2.12a}$$

$$M_\theta=B_{12}\varepsilon_{xm}+B_{22}\varepsilon_{\theta m}+D_{12}k_x+D_{22}k_\theta, \tag{2.12b}$$

$$M_{x\theta}=B_{66}\gamma_{x\theta m}+2D_{66}k_{x\theta}, \tag{2.12c}$$

and

$$Q_x=A_{44}\gamma_{xzm}=A_{44}(w_{,x}+\phi_x),\quad Q_\theta=A_{55}\gamma_{\theta zm}=A_{55}\left[\frac{1}{x\sin\beta}w_{,\theta}+\phi_\theta\right], \tag{2.13}$$

where the coefficients A_{ij}, B_{ij}, D_{ij} are given in Appendix A.

3 Equilibrium equations

The equilibrium equations for the FG porous truncated conical shells embedded in the Pasternak foundation based on FSDT, are derived [54–56]:

$$xN_{x,x}+\frac{1}{\sin\beta}N_{x\theta,\theta}+N_x-N_\theta=0, \tag{3.1a}$$

$$\frac{1}{\sin\beta}N_{\theta,\theta}+xN_{x\theta,x}+2N_{x\theta}=0, \tag{3.1b}$$

$$\begin{aligned}&xM_{x,xx}+2M_{x,x}+\frac{2}{\sin\beta}M_{x\theta,x\theta}+\frac{2}{x\sin\beta}M_{x\theta,\theta}+\frac{1}{x\sin^2\beta}M_{\theta,\theta\theta}-M_{\theta,x}-N_\theta\cot\beta\\&\quad+\left[xN_xw_{,x}+\frac{1}{\sin\beta}N_{x\theta}w_{,\theta}\right]_{,x}+\frac{1}{\sin\beta}\left[N_{x\theta}w_{,x}+\frac{1}{x\sin\beta}N_\theta w_{,\theta}\right]_{,\theta}\\&=xK_1w-xK_2\left(\frac{\partial^2w}{\partial x^2}+\frac{1}{x}\frac{\partial w}{\partial x}+\frac{1}{x^2\sin^2\beta}\frac{\partial^2w}{\partial\theta^2}\right),\end{aligned} \tag{3.1c}$$

$$(x\sin\beta M_x)_{,x}+M_{x\theta,\theta}-M_\theta\sin\beta-x\sin\beta Q_x=0, \tag{3.1d}$$

$$(x\sin\beta M_{x\theta})_{,x}+M_{\theta,\theta}+M_{x\theta}\sin\beta-x\sin\beta Q_\theta=0, \tag{3.1e}$$

where $()_{,x}$ and $()_{,\theta}$ indicate the derivatives with respect to the axial and circumferential coordinate, respectively.

4 Stability equations

Using the adjacent equilibrium criterion, the linearized stability equations associated with the onset of buckling are obtained. Based on this criterion and perturbation technique, the displacement components on the primary equilibrium path are perturbed infinitesimally to establish an adjacent equilibrium position. Therefore, there are displacement components related to the primary equilibrium path

$$u=u_0+u_1,\quad v=v_0+v_1,\quad w=w_0+w_1,\quad \phi_x=\phi_{x0}+\phi_{x1},\quad \phi_\theta=\phi_{\theta0}+\phi_{\theta1}, \tag{4.1}$$

where the displacement components with subscript 1 are infinitesimal and nonzero displacements.

Analogously, for the force and moment resultants of a neighboring state may be associated with the state of equilibrium also are of the form

$$N_x=N_{x0}+N_{x1},\quad N_\theta=N_{\theta0}+N_{\theta1},\quad N_{x\theta}=N_{x\theta0}+N_{x\theta1},\quad Q_x=Q_{x0}+Q_{x1}, \tag{4.2a}$$

$$Q_\theta=Q_{\theta0}+Q_{\theta1},\quad M_x=M_{x0}+M_{x1},\quad M_\theta=M_{\theta0}+M_{\theta1},\quad M_{x\theta}=M_{x\theta0}+M_{x\theta1}. \tag{4.2b}$$

After substituting the above equation into Eqs. (3.1a)-(3.1e), the incremental values of stress resultants are obtained. Since the incremental displacements are small enough, the

stability equations associated with the equilibrium Eqs. (3.1a)-(3.1e) are obtained as

$$xN_{x1,x}+\frac{1}{\sin\alpha}N_{x\theta1,\theta}+N_{x1}-N_{\theta1}=0, \tag{4.3a}$$

$$\frac{1}{\sin\alpha}N_{\theta1,\theta}+xN_{x\theta1,x}+2N_{x\theta1}=0, \tag{4.3b}$$

$$\begin{aligned}&xM_{x1,xx}+2M_{x1,x}+\frac{2}{\sin\alpha}M_{x\theta1,x\theta}+\frac{2}{x\sin\alpha}M_{x\theta1,\theta}+\frac{1}{x\sin^2\alpha}M_{\theta1,\theta\theta}-M_{\theta1,x}-N_{\theta1}\cot\alpha\\&\quad+\left[xN_{x0}w_{1,x}+\frac{1}{\sin\alpha}N_{x\theta0}w_{1,\theta}\right]_{,x}+\frac{1}{\sin\alpha}\left[N_{x\theta0}w_{1,x}+\frac{1}{x\sin\alpha}N_{\theta0}w_{1,\theta}\right]_{,\theta}\\&=xK_1w-xK_2\left(\frac{\partial^2w}{\partial x^2}+\frac{1}{x}\frac{\partial w}{\partial x}+\frac{1}{x^2\sin^2\beta}\frac{\partial^2w}{\partial\theta^2}\right),\end{aligned} \tag{4.3c}$$

$$x\sin\alpha M_{x1,x}+\sin\alpha M_{x1}+M_{x\theta1,\theta}-M_{\theta1}\sin\alpha-x\sin\alpha Q_{x1}=0, \tag{4.3d}$$

$$x\sin\alpha M_{x\theta1,x}+2\sin\alpha M_{x\theta1}+M_{\theta1,\theta}-x\sin\alpha Q_{\theta1}=0, \tag{4.3e}$$

where

$$N_{x1}=A_{11}\varepsilon_{xm1}+A_{12}\varepsilon_{\theta m1}+B_{11}k_{x1}+B_{12}k_{\theta1},\quad N_{\theta1}=A_{12}\varepsilon_{xm1}+A_{22}\varepsilon_{\theta m1}+B_{12}k_{x1}+B_{22}k_{\theta1}, \tag{4.4a}$$

$$N_{x\theta1}=A_{66}\gamma_{x\theta m1}+2B_{66}k_{x\theta1},\quad M_{x1}=B_{11}\varepsilon_{xm1}+B_{12}\varepsilon_{\theta m1}+D_{11}k_{x1}+D_{12}k_{\theta1}, \tag{4.4b}$$

$$M_{\theta1}=B_{12}\varepsilon_{xm1}+B_{22}\varepsilon_{\theta m1}+D_{12}k_{x1}+D_{22}k_{\theta1},\quad M_{x\theta1}=B_{66}\gamma_{x\theta m1}+2D_{66}k_{x\theta1}, \tag{4.4c}$$

$$Q_{x1}=A_{44}\gamma_{xzm1}=A_{44}(w_{1,x}+\phi_{x1}),\quad Q_{\theta1}=A_{55}\gamma_{\theta zm1}=A_{55}\left[\frac{1}{x\sin\alpha}w_{1,\theta}+\phi_{\theta1}\right], \tag{4.4d}$$

and the linear forms of strains and curvatures, and twist in terms of the displacement components are given as

$$\varepsilon_{xm1}=u_{1,x},\quad \varepsilon_{\theta m1}=\frac{1}{x\sin\alpha}v_{1,\theta}+\frac{u_1}{x}+\frac{w_1}{x}\cot\alpha,\quad \gamma_{x\theta m1}=\frac{1}{x\sin\alpha}u_{1,\theta}-\frac{v_1}{x}+v_{1,x}, \tag{4.5a}$$

$$\gamma_{xzm1}=w_{1,x}+\phi_{x1},\quad \gamma_{\theta zm1}=\frac{1}{x\sin\alpha}w_{1,\theta}+\phi_{\theta1},\quad k_{x1}=\phi_{x1,x}, \tag{4.5b}$$

$$k_{\theta1}=\frac{1}{x\sin\alpha}\phi_{\theta1,\theta}+\frac{1}{x}\phi_{x1},\quad k_{x\theta1}=\frac{1}{2}\left[\phi_{\theta1,x}+\frac{1}{x\sin\alpha}\phi_{x1,\theta}-\frac{1}{x}\phi_{\theta1}\right]. \tag{4.5c}$$

Eq. (4.3) are stability equations of an FG porous truncated conical shells. In Eq. (4.3) the subscript 0 deals with the equilibrium state and subscript 1 deals with the stability state. The terms with the subscript 0 are the solution of the equilibrium equations for the given load.

5 Mechanical buckling analysis of an FG porous truncated conical shell

5.1 Derivations

For this aim, assuming that FG porous truncated conical shells is subjected to the axial compressive load of intensity $p(N)$ at $x=x_0$. As can be seen in Eq. (4.3), there are pre-

buckling force resultants. By solving the membrane form of the equilibrium equations, the prebuckling force resultants are determined as

$$N_{x0}=-\frac{px_0}{x\cos\beta},\quad N_{\theta 0}=0,\quad N_{x\theta 0}=0. \tag{5.1}$$

Substituting Eqs. (4.4)-(5.1) into Eq. (4.3), we get nonlinear stability equations of a FG porous truncated conical shell in terms of displacement components u_1, v_1, w_1 and ϕ_{x1}, $\phi_{\theta 1}$ as follows

$$R_{11}(u_1)+R_{12}(v_1)+R_{13}(w_1)+R_{14}(\phi_{x1})+R_{15}(\phi_{\theta 1})=0, \tag{5.2a}$$
$$R_{21}(u_1)+R_{22}(v_1)+R_{23}(w_1)+R_{24}(\phi_{x1})+R_{25}(\phi_{\theta 1})=0, \tag{5.2b}$$
$$R_{31}(u_1)+R_{32}(v_1)+(R_{33}+PR_{36}+R_{37}K_1+R_{38}K_2)(w_1)+R_{34}(\phi_{x1})+R_{35}(\phi_{\theta 1})=0, \tag{5.2c}$$
$$R_{41}(u_1)+R_{42}(v_1)+R_{43}(w_1)+R_{44}(\phi_{x1})+R_{45}(\phi_{\theta 1})=0, \tag{5.2d}$$
$$R_{51}(u_1)+R_{52}(v_1)+R_{53}(w_1)+R_{54}(\phi_{x1})+R_{55}(\phi_{\theta 1})=0, \tag{5.2e}$$

where $P=2\pi px_0\sin\beta$ and R_{ij} are differential operators that are defined in Appendix B.

5.2 Solution procedure

A FG porous truncated conical shells is considered. Its boundary edges are simply supported and the boundary conditions are [22]

$$N_{x1}=v_1=w_1=\phi_{\theta 1}=M_{x1}=0 \quad \text{at} \quad x=x_0,x_0+L. \tag{5.3}$$

The solution for five Eqs. (5.2a)-(5.2e), satisfying the boundary conditions given by Eq. (5.3), may be assumed as [24,25]

$$u=U\cos\frac{m\pi(x-x_0)}{L}\sin n\theta, \qquad v=V\sin\frac{m\pi(x-x_0)}{L}\cos n\theta, \tag{5.4a}$$
$$w=W\sin\frac{m\pi(x-x_0)}{L}\sin n\theta, \qquad \phi_x=\Phi_1\cos\frac{m\pi(x-x_0)}{L}\sin n\theta, \tag{5.4b}$$
$$\phi_\theta=\Phi_2\frac{1}{x\sin\beta}\sin\frac{m\pi(x-x_0)}{L}\cos n\theta, \tag{5.4c}$$

where m, n are the number of half-waves in the generatrix direction and the number of full-waves in the circumferential direction of the shell. In Eq. (5.5), U, V, W, and Φ_1, Φ_2 are constant coefficients. Substituting Eq. (5.5) into Eqs. (5.2a)-(5.2e), then using the Galerkin's method, we have equations

$$X_{11}U+X_{12}V+X_{13}W+X_{14}\Phi_1+X_{15}\Phi_2=0, \tag{5.5a}$$
$$X_{21}U+X_{22}V+X_{23}W+X_{24}\Phi_1+X_{25}\Phi_2=0, \tag{5.5b}$$
$$X_{31}U+X_{32}V+(R_{33}+PR_{36}+R_{37}K_1+R_{38}K_2)W+X_{34}\Phi_1+X_{35}\Phi_2=0, \tag{5.5c}$$
$$X_{41}U+X_{42}V+X_{43}W+X_{44}\Phi_1+X_{45}\Phi_2=0, \tag{5.5d}$$
$$X_{51}U+X_{52}V+X_{53}W+X_{54}\Phi_1+X_{55}\Phi_2=0. \tag{5.5e}$$

Herein, the coefficients X_{ij} are constants which are calculated in Appendix C. To get the mechanical buckling force for the FG porous truncated conical shells, the coefficient matrix of algebraic Eqs. (5.5a)-(5.5e) must be set equal to zero as

$$\begin{vmatrix} X_{11} & X_{12} & X_{13} & X_{14} & X_{15} \\ X_{21} & X_{22} & X_{23} & X_{24} & X_{25} \\ X_{31} & X_{32} & (R_{33}+PR_{36}+R_{37}K_1+R_{38}K_2) & X_{34} & X_{35} \\ X_{41} & X_{42} & X_{43} & X_{44} & X_{45} \\ X_{51} & X_{52} & X_{53} & X_{54} & X_{55} \end{vmatrix} = 0. \tag{5.6}$$

Expanding this determinant and solving the resulting equation for the combination of P yields

$$PX_{37} = -X_{31}\frac{D_1}{D_3} + X_{32}\frac{D_2}{D_3} + X_{34}\frac{D_4}{D_3} - X_{35}\frac{D_5}{D_3} - X_{33} - R_{37}K_1 - R_{38}K_2, \tag{5.7}$$

where D_i $(i=1,2,3,4,5)$ are calculated by

$$D_1 = \begin{vmatrix} X_{12} & X_{13} & X_{14} & X_{15} \\ X_{22} & X_{23} & X_{24} & X_{25} \\ X_{42} & X_{43} & X_{44} & X_{45} \\ X_{52} & X_{53} & X_{54} & X_{55} \end{vmatrix}, \qquad D_2 = \begin{vmatrix} X_{11} & X_{13} & X_{14} & X_{15} \\ X_{21} & X_{23} & X_{24} & X_{25} \\ X_{41} & X_{43} & X_{44} & X_{45} \\ X_{51} & X_{53} & X_{54} & X_{55} \end{vmatrix}, \tag{5.8a}$$

$$D_3 = \begin{vmatrix} X_{11} & X_{12} & X_{14} & X_{15} \\ X_{21} & X_{22} & X_{24} & X_{25} \\ X_{41} & X_{42} & X_{44} & X_{45} \\ X_{51} & X_{52} & X_{54} & X_{55} \end{vmatrix}, \qquad D_4 = \begin{vmatrix} X_{11} & X_{12} & X_{13} & X_{15} \\ X_{21} & X_{22} & X_{23} & X_{25} \\ X_{41} & X_{42} & X_{43} & X_{45} \\ X_{51} & X_{52} & X_{53} & X_{55} \end{vmatrix}, \tag{5.8b}$$

$$D_5 = \begin{vmatrix} X_{11} & X_{12} & X_{13} & X_{14} \\ X_{21} & X_{22} & X_{23} & X_{24} \\ X_{41} & X_{42} & X_{43} & X_{44} \\ X_{51} & X_{52} & X_{53} & X_{54} \end{vmatrix}. \tag{5.8c}$$

Eq. (5.7) is an expression used to determine the critical buckling loads P_{cr} for the FG porous truncated conical shells P_{cr} subjected to axial compressive load.

5.3 Numerical results and discussion

5.3.1 Comparison results

To validate proposed approach, we consider a simply supported isotropic truncated conical shells only under axial compressive load in the absence of elastic foundations. Critical buckling loads of shell are calculated by using explicit expression (5.7) and compared in Table 1 with those reported by Naj et al. [17] and Baruch et al. [53]. The comparisons for the shell with the material and shell properties are as follows: $k=0$, $h=0.01$m, $R=100\times h$, $\nu=0.3$, $P^*=P_{cr}/P_{cl}$, where $P_{cl}=\frac{2\pi Eh^2\cos^2\alpha}{\sqrt{3(1-\nu^2)}}$ [17]. It is evident that an excellent agreement.

Table 1: Comparisons with results of [17] and [53] for an isotropic truncated cone. * Buckling mode (m,n).

β	$L/R=0.2$			$L/R=0.5$		
	[17]	[53]	P* (Present)	[17]	[53]	P* (Present)
1°	1.005(7)	1.005(7)	0.9962(1,6)*	1.0017(8)	1.002(8)	0.9979(3,1)
5°	1.006(7)	1.006(7)	0.9962 (1,6)	1.0010(8)	1.002(8)	0.9988(2,8)
10°	1.007(7)	1.007(7)	0.9962 (1,6)	1.0000(8)	1.002(8)	0.9985(2,8)
30°	1.0171(5)	1.017(5)	0.9980 (1,4)	0.9870(7)	1.001(7)	1.0000(2,7)
60°	1.148(0)	1.144(0)	1.1267 (1,1)	1.045(7)	1.044(7)	1.0140(1,7)

In the following section, the effects of shell characteristics, porosity distribution, porosity coefficient, and elastic foundation on the critical buckling load of a FG porous truncated conical shells are investigated. We consider $E_{\max}=200.10^9\text{N/m}^2$, $\nu=0.3$, the geometrical parameters are $h=0.025$m, $R=40\times h$; $L=2\times R$, $\beta=15^\circ$ and $K_1=2.5\times10^7\text{N/m}^3$, $K_2=2.5\times10^5\text{N/m}$.

5.3.2 Effect of the R/h and L/R ratios

In this section, the effects of R/h and L/R ratios on the critical buckling load P_{cr} of a FG porous truncated conical shells with symmetric porosity distribution, non-symmetric porosity distribution, and uniform porosity distribution, respectively, are presented in Table 2 and Table 3 and Fig. 3. Clearly, for different cases, critical buckling loads P_{cr} of Type 1 is the largest among all the porosity distributions, Type 2 is the second and Type 3 is the smallest. Moreover, the critical buckling load P_{cr} strongly decreases when R/h ratio increases. For example, in Table 2, the critical buckling load P_{cr} of a FG porous truncated conical shells decreases from 6239.40MN to 66.072MN as R/h increases from 10 to 100 for the Type 1. It means that the thinner the shell is, the smaller the value of the critical buckling load will be. The ratio R/h has a significant influence on the value of the critical buckling load P_{cr}, but the ratio R/L has a negligible effect on the value of the critical buckling load P_{cr} as shown in Table 3.

Table 2: Effect of the R/h on the critical buckling load P_{cr}. * Buckling mode (m,n).

R/h	5	10	20	50	100	200	500
Type 1	24394.000	6239.400	1585.700	258.120	66.072	17.643	3.9251
	(2,2)*	(3,2)	(4,3)	(7,1)	(10,1)	(14,1)	(23,1)
Type 2a	23741.000	6072.600	1543.800	251.386	64.354	17.2199	3.8519
	(2,2)	(3,2)	(4,3)	(7,2)	(10,1)	(14,1)	(23,1)
Type 2b	23747.000	6074.700	1544.100	251.460	64.373	17.2244	3.8526
	(2,2)	(3,2)	(4,3)	(7,2)	(10,1)	(14,1)	(23,1)
Type 3	23579.000	6031.700	1533.400	249.699	63.932	17.1151	3.8343
	(2,2)	(3,2)	(4,3)	(7,2)	(10,1)	(14,1)	(23,1)

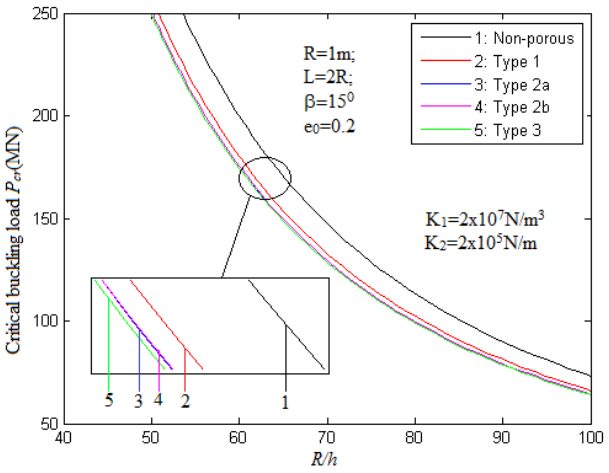

Figure 3: Effects of the R/h ratio on the critical buckling load P_{cr}.

Table 3: Effect of the L/R on the critical buckling load P_{cr}. * Buckling mode (m,n).

L/R	0.2	0.5	1	1.5	2	3	5
Type 1	491.419	404.557	399.661	400.841	401.504	403.715	408.3771
	(1,1)*	(3,2)	(3,4)	(5,1)	(6,3)	(8,4)	(11,6)
Type 2a	471.940	393.463	389.056	389.892	390.920	393.3101	397.3789
	(1,1)	(1,6)	(3,4)	(5,1)	(6,3)	(8,4)	(11,6)
Type 2b	471.962	393.478	389.089	389.991	391.010	393.3921	397.399
	(1,1)	(1,6)	(3,4)	(5,1)	(6,3)	(8,4)	(11,6)
Type 3	467.737	390.692	386.398	387.218	388.294	390.7032	394.6522
	(1,1)	(1,6)	(3,4)	(5,1)	(6,3)	(8,4)	(11,6)

5.3.3 Effect of angle β

The effect of semi-vertex angle β on the critical buckling load P_{cr} of a FG porous truncated conical shells is presented in Table 4 and Figs. 4-8. From these illustrations, we see that the critical buckling load P_{cr} decreases when the semi-vertex angle β increases for both three types of the porosity distributions.

5.3.4 Effect of different porosity coefficients e_0 for various porosity distributions

The influence of different porosity distribution types on the critical buckling load P_{cr} of a FG porous truncated conical shells with the same porosity coefficient is presented in Fig. 8. The porosity coefficient $e_0=0.2$ is chosen while holding all other fixed parameters. It is clear that the Type 1 (symmetric porosity distribution) occupies more stiffness feature when compared with other two types. Thus the critical buckling loads of Type 1 is bigger than those of Type 2 and Type 3.

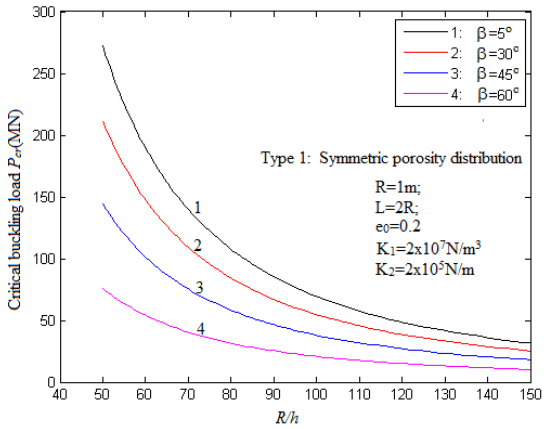

Figure 4: Effects of semi-vertex angle β on the critical buckling load P_{cr} for Type 1.

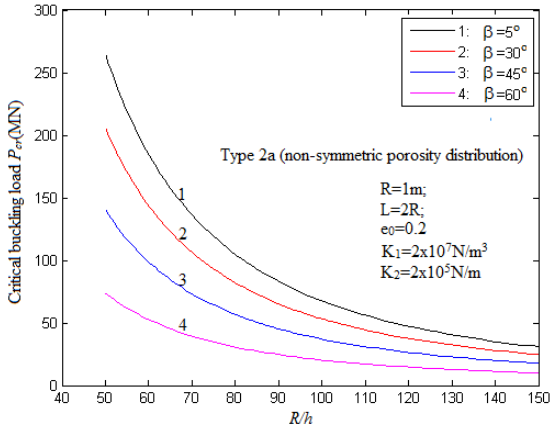

Figure 5: Effects of semi-vertex angle β on the critical buckling load P_{cr} for Type 2a.

Table 4: Effect of semi-vertex angle β on the critical buckling load P_{cr}. * Buckling mode (m,n).

β	1	5	10	15	30	45	60
Type 1	424.935	422.811	415.829	401.504	328.044	223.399	117.6459
	(7,2)*	(7,1)	(6,4)	(6,3)	(5,3)	(4,4)	(3,4)
Type 2a	414.131	411.769	404.741	390.920	319.484	217.5449	114.757
	(7,2)	(7,1)	(6,4)	(6,3)	(5,4)	(4,4)	(3,4)
Type 2b	414.132	411.791	404.768	391.010	319.620	217.6941	114.8547
	(7,2)	(7,1)	(6,4)	(6,3)	(5,4)	(4,4)	(3,4)
Type 3	411.349	408.972	401.964	388.294	317.322	216.1622	114.0835
	(7,2)	(7,1)	(6,4)	(6,3)	(5,4)	(4,4)	(3,4)

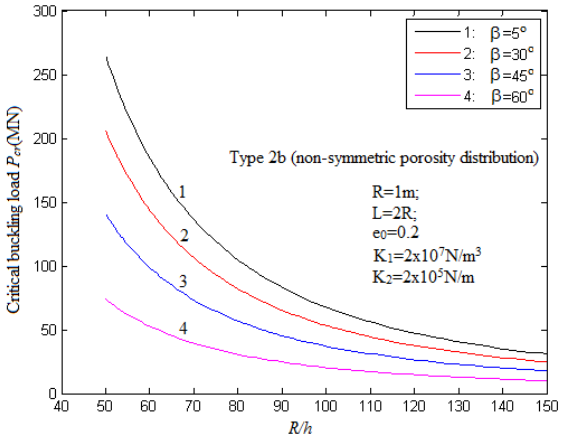

Figure 6: Effects of semi-vertex angle β on the critical buckling load P_{cr} for Type 2b.

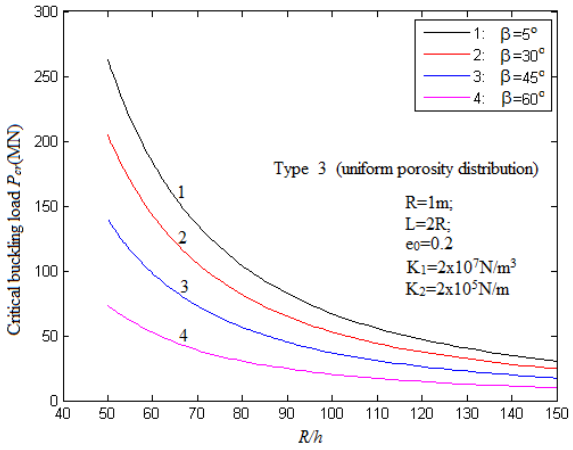

Figure 7: Effects of semi-vertex angle β on the critical buckling load P_{cr} for Type 3.

The effects of porosity coefficients e_0 on the critical buckling load P_{cr} of a FG porous truncated conical shells for different porosity coefficients with symmetric porosity distribution, non-symmetric porosity distribution, and uniform porosity distribution, respectively, are tabulated in Table 5 and plotted in Figs. 9-12. They show that by increasing the value of the coefficient of porosity e_0, the critical buckling load P_{cr} decreases for all types of the porosity distribution. For example, in Table 5, the critical buckling load P_{cr} of a FG porous truncated conical shells decreases from 34% to 51.3%, as e_0 increases from 0.2 to 0.8. This observation can be explained as because the increase of the porosity coefficients leads to the decrease of stiffness of shell.

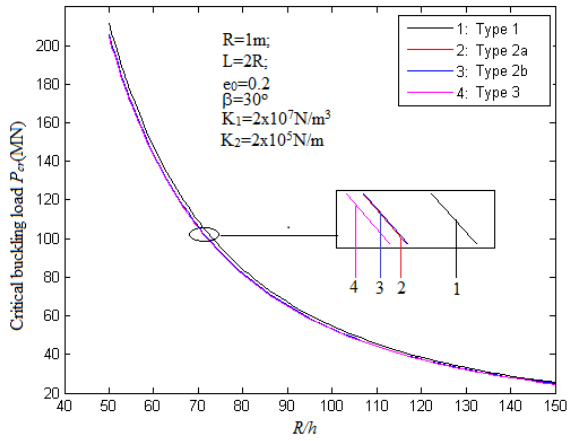

Figure 8: Effects of different porosity distribution types on the critical buckling loads P_{cr}.

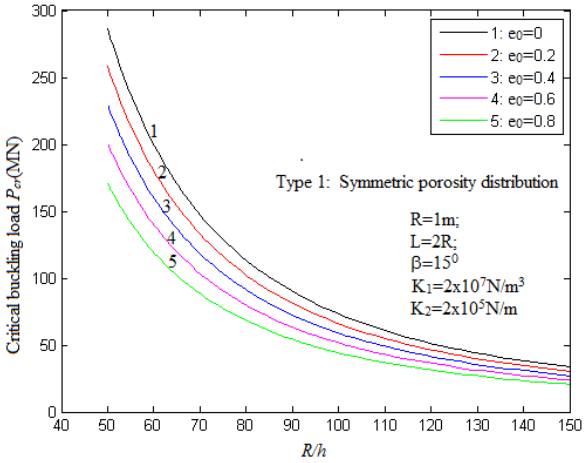

Figure 9: Effect of porosity coefficients e_0 on the critical buckling load P_{cr} for Type 1.

5.3.5 Effect of elastic foundations

Table 6 shows the influence of foundations on the critical buckling load P_{cr} a FG porous truncated conical shell with different porosity distribution types. It was found that the critical buckling loads P_{cr} increase when the elastic foundation parameters K_1 and K_2 increase separately or together. In addition, the elastic foundation increases the load-carrying capability of the shell.

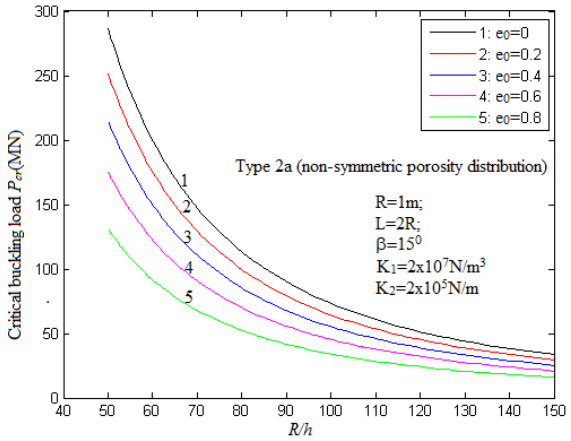

Figure 10: Effect of porosity coefficients e_0 on the critical buckling load P_{cr} for Type 2a.

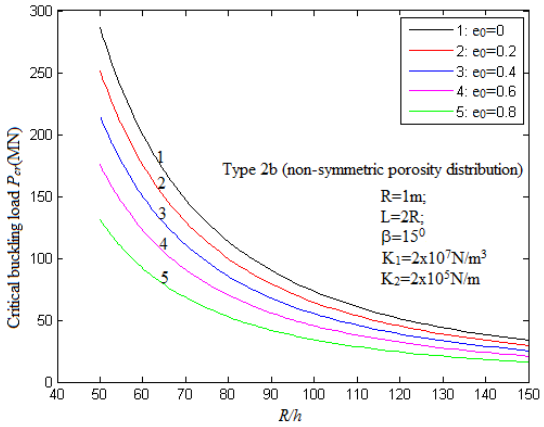

Figure 11: Effect of porosity coefficients e_0 on the critical buckling load P_{cr} for Type 2b.

Table 5: Effect of porosity coefficients e_0 on the critical buckling load P_{cr}. * Buckling mode (m,n).

e_0	0.2	0.3	0.4	0.5	0.6	0.7	0.8
Type 1	401.504	379.123	356.548	333.961	311.051	288.115	265.123
	(6,3)*	(6,2)	(6,2)	(6,2)	(6,1)	(6,1)	(5,4)
Type 2a	390.920	362.661	333.643	303.654	272.391	239.411	203.4324
	(6,3)	(6,3)	(6,3)	(6,3)	(6,3)	(6,3)	(6,4)
Type 2b	391.010	362.796	333.823	303.878	272.660	239.7255	203.6661
	(6,3)	(6,3)	(6,3)	(6,3)	(6,3)	(6,3)	(6,4)
Type 3	388.294	358.551	327.929	296.196	262.998	227.7373	189.2486
	(6,3)	(6,3)	(6,3)	(6,3)	(6,3)	(6,3)	(6,3)

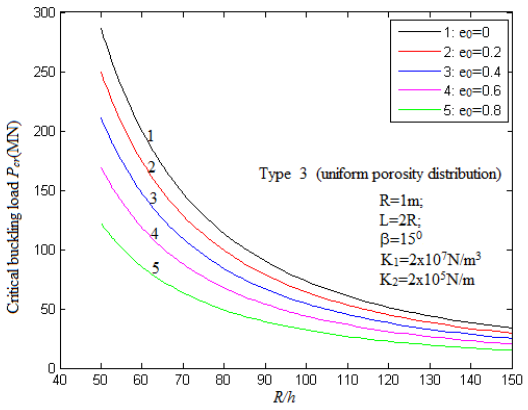

Figure 12: Effect of porosity coefficients e_0 on the critical buckling load P_{cr} for Type 3.

Table 6: Effect of elastic foundations on the critical buckling load P_{cr}. * Buckling mode (m,n).

Type 1	$K_2=0$N/m	$K_2=10^5$N/m	$K_2=2\times10^5$N/m	$K_2=5\times10^5$N/m
$K_1=0$N/m^3	397.3231(5,5)*	-	-	-
$K_1=10^7$N^3	398.6111(5,5)	399.5966(5,5)	400.5821(5,5)	403.1122(6,3)
$K_1=2\times10^7$N^3	399.7929(6,3)	400.6357(6,3)	401.4785(6,3)	404.0069(6,3)
$K_1=5\times10^7$N^3	402.4769(6,3)	403.3197(6,3)	404.1625(6,3)	406.6909(6,3)
Type 2a	$K_2=0$N/m	$K_2=10^5$N/m	$K_2=2\times10^5$N/m	$K_2=5\times10^5$N/m
$K_1=0$N^3	387.2294(5,5)*	-	-	-
$K_1=10^7$N^3	388.3139(6,3)	389.1567(6,3)	389.9995(6,3)	389.9018(6,3)
$K_1=2\times10^7$N^3	389.2085(6,3)	390.0513(6,3)	390.8941(6,3)	393.4226(6,3)
$K_1=5\times10^7$N^3	391.8926(6,3)	392.7354(6,3)	393.5782(6,3)	396.1066(6,3)
Type 2b	$K_2=0$N/m	$K_2=10^5$N/m	$K_2=2\times10^5$N/m	$K_2=5\times10^5$N/m
$K_1=0$N^3	387.2434(5,5)*	-	-	-
$K_1=10^7$N^3	388.4037(6,3)	389.2465(6,3)	390.0893(6,3)	392.6177(6,3)
$K_1=2\times10^7$N^3	389.2984(6,3)	390.1412(6,3)	390.9840(6,3)	393.5124(6,3)
$K_1=5\times10^7$N^3	391.9825(6,3)	392.8253(6,3)	393.6681(6,3)	396.1965(6,3)
Type 3	$K_2=0$N/m	$K_2=10^5$N/m	$K_2=2\times10^5$N/m	$K_2=5\times10^5$N/m
$K_1=0$N^3	384.6328(5,5)*	-	-	-
$K_1=10^7$N^3	385.6877(6,3)	386.5305(6,3)	387.3733(6,3)	403.1122(6,3)
$K_1=2\times10^7$N^3	386.5824(6,3)	387.4252(6,3)	388.2680(6,3)	390.7964(6,3)
$K_1=5\times10^7$N^3	389.2665(6,3)	390.1093(6,3)	390.9521(6,3)	393.4805(6,3)

6 Conclusions

In this research, the buckling of a FG porous truncated conical shells resting on the Winkler–Pasternak foundation and subjected to a uniform axial compressive load has been investigated. Three types of FG porous distributions including symmetric porosity dis-

tribution, non-symmetric porosity stiff or soft distribution and uniform porosity distribution are considered. The stability equations for the shell are derived based on the first order shear deformation theory. Those equations are solved by the Galerkin method to determine the expression of the critical buckling load P_{cr}. The effects of shell characteristics, porosity distribution, porosity coefficient, and elastic foundation on the critical buckling load were discussed in details. Comparing the results of this study with those in the literature validates the present analysis.

Appendix A

$$A_{11}=A_{22}=\frac{E_1}{1-\nu^2}, \qquad A_{12}=\frac{\nu E_1}{1-\nu^2},$$
$$A_{44}=A_{55}=\frac{5E_1}{12(1+\nu)}, \qquad A_{66}=\frac{E_1}{2(1+\nu)},$$
$$B_{11}=B_{22}=\frac{E_2}{1-\nu^2}, \qquad B_{12}=\frac{\nu E_2}{1-\nu^2},$$
$$B_{66}=\frac{E_2}{2(1+\nu)}, \qquad D_{11}=D_{22}=\frac{E_3}{1-\nu^2},$$
$$D_{12}=\frac{\nu E_3}{1-\nu^2}, \qquad D_{66}=\frac{E_3}{2(1+\nu)}.$$

For FG porous truncated conical shell with porous distributions:

Type 1 (symmetric porosity distribution)

$$E_1=\frac{E_{\max}h(\pi-2e_0)}{\pi}, \quad E_2=0, \quad E_3=\frac{E_{\max}h^3\left(48e_0-6e_0\pi^2+\pi^3\right)}{12\pi^3}.$$

Type 2 (non-symmetric porosity distribution)

$$\text{Type 2a}: \quad E_1=\frac{E_{\max}h(\pi-2e_0)}{\pi}, \qquad E_2=\frac{E_{\max}e_0h^2(\pi-4)}{\pi^2},$$
$$E_3=\frac{E_{\max}h^3}{12\pi^3}\left[\pi^3-6e_0\pi^2+(192-48\pi)e_0\right],$$
$$\text{Type 2b}: \quad E_1=\frac{E_{\max}h(\pi-2e_0)}{\pi}, \qquad E_2=-\frac{E_{\max}e_0h^2(\pi-4)}{\pi^2},$$
$$E_3=\frac{E_{\max}h^3}{12\pi^3}\left[\pi^3-6e_0\pi^2+(192-48\pi)e_0\right].$$

Type 3 (uniform porosity distribution)

$$E_1=E_{\max}(1-e_0\lambda)h, \quad E_2=0, \quad E_3=\frac{E_{\max}(1-e_0\lambda)h^3}{12}.$$

Appendix B

In Eqs. (5.2a)-(5.2e):

$$
\begin{aligned}
R_{11} &= xA_{11}\frac{\partial^2}{\partial x^2}+\frac{A_{66}}{x(\sin\beta)^2}\frac{\partial^2}{\partial y^2}+A_{11}\frac{\partial}{\partial x}-A_{22}\frac{1}{x},\\
R_{12} &= \frac{1}{\sin\beta}(A_{12}+A_{66})\frac{\partial^2}{\partial x\partial\theta}-\frac{1}{x\sin\beta}(A_{22}+A_{66})\frac{\partial}{\partial\theta},\\
R_{13} &= \cot\beta A_{12}\frac{\partial}{\partial x}-A_{22}\cot\beta\frac{1}{x},\\
R_{14} &= B_{11}x\frac{\partial^2}{\partial x^2}+\frac{1}{x\sin^2\beta}B_{66}\frac{\partial^2}{\partial\theta^2}+B_{11}\frac{\partial}{\partial x}-B_{22}\frac{1}{x},\\
R_{15} &= \frac{1}{\sin\beta}(B_{12}+B_{66})\frac{\partial^2}{\partial x\partial\theta}-\frac{1}{x\sin\beta}(B_{22}+B_{66})\frac{\partial}{\partial\theta},\\
R_{21} &= \frac{1}{\sin\beta}(A_{12}+A_{66})\frac{\partial^2}{\partial x\partial\theta}+\frac{1}{x\sin\beta}(A_{22}+A_{66})\frac{\partial}{\partial\theta},\\
R_{22} &= A_{66}x\frac{\partial^2}{\partial x^2}+\frac{A_{22}}{x\sin^2\beta}\frac{\partial^2}{\partial\theta^2}+A_{66}\frac{\partial}{\partial x}-A_{66}\frac{1}{x},\\
R_{23} &= \frac{A_{22}}{x\sin\beta}\cot\beta\frac{\partial}{\partial\theta},\\
R_{24} &= \frac{1}{\sin\beta}(B_{12}+B_{66})\frac{\partial^2}{\partial x\partial\theta}+\frac{1}{x\sin\beta}(B_{22}+B_{66})\frac{\partial}{\partial\theta},\\
R_{25} &= B_{66}x\frac{\partial^2}{\partial x^2}+\frac{B_{22}}{x\sin^2\beta}\frac{\partial^2}{\partial\theta^2}+B_{66}\frac{\partial}{\partial x}-B_{66}\frac{1}{x},\\
R_{31} &= B_{11}x\frac{\partial^3}{\partial x^3}+\frac{1}{x\sin^2\beta}(B_{12}+2B_{66})\frac{\partial^3}{\partial x\partial\theta^2}+2B_{11}\frac{\partial^2}{\partial x^2}+\frac{B_{22}}{x^2\sin^2\beta}\frac{\partial^2}{\partial\theta^2}\\
&\quad-\left(A_{12}\cot\beta+B_{22}\frac{1}{x}\right)\frac{\partial}{\partial x}-\left(A_{22}\cot\beta-B_{22}\frac{1}{x}\right)\frac{1}{x},\\
R_{32} &= (B_{12}+2B_{66})\frac{1}{\sin\beta}\frac{\partial^3}{\partial x^2\partial\theta}+B_{22}\frac{1}{x^2\sin^3\beta}\frac{\partial^3}{\partial\theta^3}-B_{22}\frac{1}{x\sin\beta}\frac{\partial^2}{\partial x\partial\theta}\\
&\quad-\left(A_{22}\cot\beta-B_{22}\frac{1}{x}\right)\frac{1}{x\sin\beta}\frac{\partial}{\partial\theta},\\
R_{33} &= B_{12}\cot\beta\frac{\partial^2}{\partial x^2}+B_{22}\cot\beta\frac{1}{x^2\sin^2\beta}\frac{\partial^2}{\partial\theta^2}-B_{22}\cot\beta\frac{1}{x}\frac{\partial}{\partial x}-\left(A_{22}\cot\beta-B_{22}\frac{1}{x}\right)\cot\beta\frac{1}{x},\\
R_{34} &= D_{11}x\frac{\partial^3}{\partial x^3}+\frac{1}{x\sin^2\beta}(D_{12}+2D_{66})\frac{\partial^3}{\partial x\partial\theta^2}+2D_{11}\frac{\partial^2}{\partial x^2}+D_{22}\frac{1}{x^2\sin^2\beta}\frac{\partial^2}{\partial\theta^2}\\
&\quad-\left(B_{12}\cot\beta+D_{22}\frac{1}{x}\right)\frac{\partial}{\partial x}-\left(B_{22}\cot\beta-D_{22}\frac{1}{x}\right)\frac{1}{x},
\end{aligned}
$$

$$R_{35}=(D_{12}+2D_{66})\frac{1}{\sin\beta}\frac{\partial^3}{\partial x^2\partial\theta}+D_{22}\frac{1}{x^2\sin^3\beta}\frac{\partial^3}{\partial\theta^3}-D_{22}\frac{1}{x\sin\beta}\frac{\partial^2}{\partial x\partial\theta}$$
$$-\left(B_{22}\cot\beta-D_{22}\frac{1}{x}\right)\frac{1}{x\sin\beta}\frac{\partial}{\partial\theta},$$
$$R_{36}=-\frac{x_0}{\cos\beta}\frac{\partial^2}{\partial x^2},\quad R_{37}=-x,\quad R_{38}=x\frac{\partial^2}{\partial x^2}+\frac{1}{x\sin^2\beta}\frac{\partial^2}{\partial\theta^2}+\frac{\partial}{\partial x},$$
$$R_{41}=B_{11}x\sin\beta\frac{\partial^2}{\partial x^2}+B_{66}\frac{1}{x\sin\beta}\frac{\partial^2}{\partial\theta^2}+B_{11}\sin\beta\frac{\partial}{\partial x}-B_{22}\sin\beta\frac{1}{x},$$
$$R_{42}=(B_{12}+B_{66})\frac{\partial^2}{\partial x\partial\theta}-(B_{22}+B_{66})\frac{1}{x}\frac{\partial}{\partial\theta},$$
$$R_{43}=(B_{12}\cos\beta-A_{44}x\sin\beta)\frac{\partial}{\partial x}-B_{22}\cos\beta\frac{1}{x},$$
$$R_{44}=D_{11}x\sin\beta\frac{\partial^2}{\partial x^2}+\frac{1}{x\sin\beta}D_{66}\frac{\partial^2}{\partial\theta^2}+D_{11}\sin\beta\frac{\partial}{\partial x}-\left(A_{44}x+D_{22}\frac{1}{x}\right)\sin\beta,$$
$$R_{45}=(D_{12}+D_{66})\frac{\partial^2}{\partial x\partial\theta}-(D_{22}+D_{66})\frac{1}{x}\frac{\partial}{\partial\theta},$$
$$R_{51}=(B_{12}+B_{66})\frac{\partial^2}{\partial x\partial\theta}+(B_{22}+B_{66})\frac{1}{x}\frac{\partial}{\partial\theta},$$
$$R_{52}=B_{66}x\sin\beta\frac{\partial^2}{\partial x^2}+\frac{B_{22}}{x\sin\beta}\frac{\partial^2}{\partial\theta^2}+B_{66}\sin\beta\frac{\partial}{\partial x}-B_{66}\sin\beta\frac{1}{x},$$
$$R_{53}=-\left(A_{55}-B_{22}\cot\beta\frac{1}{x}\right)\frac{\partial}{\partial\theta},$$
$$R_{54}=(D_{12}+D_{66})\frac{\partial^2}{\partial x\partial\theta}+(D_{22}+D_{66})\frac{1}{x}\frac{\partial}{\partial\theta},$$
$$T_{55}=D_{66}x\sin\beta\frac{\partial^2}{\partial x^2}+D_{22}\frac{1}{x\sin\beta}\frac{\partial^2}{\partial\theta^2}+D_{66}\sin\beta\frac{\partial}{\partial x}-\left(A_{55}x+D_{66}\frac{1}{x}\right)\sin\beta.$$

Appendix C

In Eqs. (5.5a)-(5.5e):

$$X_{11}=-\frac{\sin\beta\pi^3m^2A_{11}}{L^2}\left(\frac{(x_0+L)^4-{x_0}^4}{8}+\frac{3L^3(2x_0+L)}{8\pi^2m^2}\right)$$
$$+\frac{1}{4}\pi L(2x_0+L)\sin\beta\left(A_{11}-A_{22}-\frac{n^2A_{66}}{\sin^2\beta}\right),$$
$$X_{12}=-\frac{mn\pi^2}{L}(A_{12}+A_{66})\left[\frac{(x_0+L)^3-x_0^3}{6}+\frac{L^3}{4m^2\pi^2}\right]-\frac{nL^2}{4m}(A_{22}+A_{66}),$$

$$X_{13}=\frac{m\pi^2}{L}\cos\beta A_{12}\left[\frac{(x_0+L)^3-x_0^3}{6}+\frac{L^3}{4m^2\pi^2}\right]+A_{22}\cos\beta\frac{L^2}{4m},$$

$$X_{14}=-\frac{m^2\pi^3}{L^2}B_{11}\sin\beta\left[\frac{(x_0+L)^4-x_0^4}{8}+\frac{3L^3(2x_0+L)}{8m^2\pi^2}\right]$$
$$+\frac{\pi}{4}L(2x_0+L)\sin\beta\left(B_{11}-B_{22}-\frac{n^2B_{66}}{(\sin\beta)^2}\right),$$

$$X_{15}=-\frac{mn\pi^2}{4}\frac{1}{\sin\beta}(2x_0+L)(B_{12}+B_{66}),$$

$$X_{21}=-\frac{mn\pi^2}{L}(A_{12}+A_{66})\left[\frac{(x_0+L)^3-x_0^3}{6}-\frac{L^3}{4m^2\pi^2}\right]-\frac{nL^2}{4m}(A_{22}+A_{66}),$$

$$X_{22}=-\frac{m^2\pi^3}{L^2}A_{66}\sin\beta\left[\frac{(x_0+L)^4-x_0^4}{8}-\frac{3L^3(2x_0+L)}{8m^2\pi^2}\right]$$
$$-\frac{\pi}{4}L(2x_0+L)\sin\beta\left(\frac{n^2}{(\sin\beta)^2}A_{22}+2A_{66}\right),$$

$$X_{23}=A_{22}\frac{n\pi}{4}L(2x_0+L)\cot\beta,$$

$$X_{24}=-\frac{mn\pi^2}{L}(B_{12}+B_{66})\left[\frac{(x_0+L)^3-x_0^3}{6}-\frac{L^3}{4m^2\pi^2}\right]-\frac{nL^2}{4m}(B_{22}+B_{66}),$$

$$X_{25}=-\frac{m^2\pi^3}{L^2}B_{66}\left[\frac{(x_0+L)^3-x_0^3}{6}-\frac{L^3}{4m^2\pi^2}\right]+\frac{\pi}{4}L\left(\frac{2n^2B_{22}}{(\sin\beta)^2}-B_{66}\right),$$

$$X_{31}=\frac{m^3\pi^4}{L^3}B_{11}\sin\beta\left\{\frac{(x_0+L)^5-x_0^5}{10}+\frac{L^2\left[x_0^3-(x_0+L)^3\right]}{2m^2\pi^2}+\frac{3L^5}{4m^4\pi^4}\right\}$$
$$+\frac{m\pi^2}{L}\cos\beta A_{12}\left[\frac{(x_0+L)^4-x_0^4}{8}-\frac{3L^3(2x_0+L)}{8m^2\pi^2}\right]$$
$$\frac{m\pi^2\sin\beta}{L}\left[3B_{11}+B_{22}+\frac{n^2(B_{12}+2B_{66})}{(\sin\beta)^2}\right]\left[\frac{(x_0+L)^3-x_0^3}{6}-\frac{L^3}{4m^2\pi^2}\right]$$
$$+A_{22}\cot\beta\sin\beta\frac{L^2(2x_0+L)}{4m}+B_{22}\frac{L^2}{4m}\sin\beta\left[\frac{n^2}{\sin^2\beta}-1\right],$$

$$X_{32}=\frac{m^2n\pi^3}{L^2}(B_{12}+2B_{66})\left[\frac{(x_0+L)^4-x_0^4}{8}-\frac{3L^3(2x_0+L)}{8m^2\pi^2}\right]$$
$$+A_{22}n\pi\cot\beta\left[\frac{(x_0+L)^3-x_0^3}{6}-\frac{L^3}{4m^2\pi^2}\right]+\frac{n\pi L(2x_0+L)}{4}B_{22}\left[\frac{n^2}{\sin^2\beta}-2\right],$$

$$
\begin{aligned}
X_{33} = & -\frac{m^2\pi^3}{L^2}\cot\beta\sin\beta B_{12}\left[\frac{(x_0+L)^4-x_0^4}{8}-\frac{3L^3(2x_0+L)}{8m^2\pi^2}\right] \\
& -\pi A_{22}\cot^2\beta\sin\beta\left[\frac{(x_0+L)^3-x_0^3}{6}-\frac{L^3}{4m^2\pi^2}\right] \\
& -\frac{\pi}{4}B_{22}L(2x_0+L)\cot\beta\sin\beta\left[\frac{n^2}{\sin^2\beta}-2\right], \\
X_{34} = & \frac{m^3\pi^4}{L^3}D_{11}\sin\beta\left\{\frac{(x_0+L)^5-x_0^5}{10}+\frac{L^2\left[x_0^3-(x_0+L)^3\right]}{2m^2\pi^2}+\frac{3L^5}{4m^4\pi^4}\right\} \\
& +B_{12}\frac{m\pi^2}{L}\cot\beta\sin\beta\left[\frac{(x_0+L)^4-x_0^4}{8}-\frac{3L^3(2x_0+L)}{8m^2\pi^2}\right] \\
& +\left[\frac{m\pi^2}{L}\sin\beta(3D_{11}+D_{22})+\frac{mn^2\pi^2}{L\sin\beta}(D_{12}+2D_{66})\right]\left[\frac{(x_0+L)^3-x_0^3}{6}-\frac{L^3}{4m^2\pi^2}\right] \\
& +\frac{L^2(2x_0+L)}{4m}B_{22}\cot\beta\sin\beta+D_{22}\frac{L^2}{4m}\sin\beta\left[\frac{n^2}{\sin^2\beta}-1\right], \\
X_{35} = & \frac{m^2n\pi^3}{L^2}\frac{1}{\sin\beta}(D_{12}+2D_{66})\left[\frac{(x_0+L)^3-x_0^3}{6}-\frac{L^3}{4m^2\pi^2}\right] \\
& +\frac{n\pi}{4\sin\beta}B_{22}L(2x_0+L)\cot\beta-\frac{n\pi}{4\sin\beta}L\left[6D_{12}+12D_{66}+\left(5-\frac{2n^2}{\sin^2\beta}\right)\right], \\
X_{36} = & -\frac{m^2\pi^3}{L^2}\sin\beta\left\{\frac{(x_0+L)^5-x_0^5}{10}+\frac{L^2\left[x_0^3-(x_0+L)^3\right]}{2m^2\pi^2}+\frac{3L^5}{4m^4\pi^4}\right\} \\
& -\frac{3\pi\sin\beta}{2}\left[\frac{(x_0+L)^3-x_0^3}{6}-\frac{L^3}{4m^2\pi^2}\right], \\
X_{37} = & -\pi\sin\beta\left\{\frac{(x_0+L)^5-x_0^5}{10}+\frac{L^2\left[x_0^3-(x_0+L)^3\right]}{2m^2\pi^2}+\frac{3L^5}{4m^4\pi^4}\right\}, \\
X_{38} = & -\frac{m^2\pi^3}{L^2}\sin\beta\left\{\frac{(x_0+L)^5-x_0^5}{10}+\frac{L^2\left[x_0^3-(x_0+L)^3\right]}{2m^2\pi^2}+\frac{3L^5}{4m^4\pi^4}\right\} \\
& -\frac{\pi}{2}\left[3\sin\beta+\frac{2n^2}{\sin\beta}\right]\left[\frac{(x_0+L)^3-x_0^3}{6}+\frac{L^3}{4m^2\pi^2}\right], \\
X_{41} = & -\frac{m^2\pi^3}{L^2}B_{11}\sin^2\beta\left[\frac{(x_0+L)^4-x_0^4}{8}+\frac{3L^3(2x_0+L)}{8m^2\pi^2}\right]
\end{aligned}
$$

$$
\begin{aligned}
&+\frac{\pi}{4}\sin^2\beta L(2x_0+L)\left[B_{11}-B_{22}-\frac{n^2}{\sin^2\beta}B_{66}\right],\\
X_{42}=&-\frac{mn\pi^2}{L}\sin\beta(B_{12}+B_{66})\left[\frac{(x_0+L)^3-x_0^3}{6}+\frac{L^3}{4m^2\pi^2}\right]-\frac{nL^2}{4m}\sin\beta(B_{22}+B_{66}),\\
X_{43}=&-\frac{m\pi^2}{L}A_{44}\sin^2\beta\left[\frac{(x_0+L)^4-x_0^4}{8}+\frac{3L^3(2x_0+L)}{8m^2\pi^2}\right]\\
&+\frac{m\pi^2}{L}\sin\beta\cos\beta B_{12}\left[\frac{(x_0+L)^3-x_0^3}{6}+\frac{L^3}{4m^2\pi^2}\right]+B_{22}\frac{L^2}{4m}\sin\beta\cos\beta,\\
X_{44}=&-\pi\sin^2\beta\left[A_{44}+\frac{m^2\pi^2}{L^2}D_{11}\right]\left[\frac{(x_0+L)^4-x_0^4}{8}+\frac{3L^3(2x_0+L)}{8m^2\pi^2}\right]\\
&+\frac{\pi\sin^2\beta}{4}L(2x_0+L)\left[D_{11}-D_{22}-\frac{n^2}{\sin^2\beta}D_{66}\right],\\
X_{45}=&-\frac{mn\pi^2}{4}(D_{12}+D_{66})(2x_0+L),\\
X_{51}=&-\frac{mn\pi^2}{L}(B_{12}+B_{66})\left[\frac{(x_0+L)^3-x_0^3}{6}-\frac{L^3}{4m^2\pi^2}\right]-\frac{nL^2}{4m}(B_{22}+B_{66}),\\
X_{52}=&-\frac{m^2\pi^3}{L^2}B_{66}\sin\beta\left[\frac{(x_0+L)^4-x_0^4}{8}-\frac{3L^3(2x_0+L)}{8m^2\pi^2}\right]\\
&-\frac{\pi\sin\beta}{4}L(2x_0+L)\left(\frac{n^2}{\sin^2\beta}B_{22}+2B_{66}\right),\\
X_{53}=&-n\pi A_{55}\left[\frac{(x_0+L)^3-x_0^3}{6}-\frac{L^3}{4m^2\pi^2}\right]+\frac{n\pi}{4}B_{22}L(2x_0+L)\cot\beta,\\
X_{54}=&-\frac{mn\pi^2}{L}(D_{12}+D_{66})\left[\frac{(x_0+L)^3-x_0^3}{6}-\frac{L^3}{4m^2\pi^2}\right]-\frac{nL^2}{4m}(D_{22}+D_{66}),\\
X_{55}=&-\pi\left[A_{55}+\frac{m^2\pi^2}{L^2}D_{66}\right]\left[\frac{(x_0+L)^3-x_0^3}{6}-\frac{L^3}{4m^2\pi^2}\right]+\frac{\pi}{4}L\left(D_{66}-\frac{2n^2}{\sin^2\beta}D_{22}\right).
\end{aligned}
$$

Acknowledgements

This research is funded by Vietnam National Foundation for Science and Technology Development (NAFOSTED) under grant number 107.02-2018.324. The authors are grateful for this support.

References

[1] R. JAVAHERI, AND M. R. ESLAMI, *Thermal buckling of functionally graded plates based on higher order theory,* J. Thermal Stress, 25 (2002), pp. 603–625.

[2] M. M. NAJAFIZADEH, AND M. R. ESLAMI, *Buckling analysis of circular plates of functionally graded materials under uniform radial compression,* Int. J. Mech. Sci., 44 (2002), pp. 2479–2493.

[3] K. M. LIEW, AND S. KITIPORNCHAI, *Thermal post-buckling of laminated plates comprising functionally graded materials with temperature-dependent properties,* J. Appl. Mech., 71 (2004), pp. 839–850.

[4] H. S. SHEN, *Postbuckling analysis of axially-loaded functionally graded cylindrical shells in thermal environments,* Compos. Sci. Tech., 62 (2002), pp. 977–987.

[5] H. S. SHEN, *Postbuckling analysis of pressure-loaded functionally graded cylindrical shells in thermal environments,* Eng. Struct., 25 (2003), pp. 487–497.

[6] H. S. SHEN, *Thermal postbuckling of shear deformable FGM cylindrical shells surrounded by an elastic medium,* J. Eng. Mech., 139(8) (2013), pp. 979–991.

[7] H. HUANG, AND Q. HAN, *Nonlinear elastic buckling and postbuckling of axially compressed functionally graded cylindrical shells,* Int. J. Mech. Sci., 51 (2009), pp. 500–507.

[8] N. D. DUC, *Nonlinear thermal dynamic analysis of eccentrically stiffened S-FGM circular cylindrical shells surrounded on elastic foundations using the Reddy's third-order shear deformation shell theory,* Euro. J. Mech. A Solids, 58 (2016), pp. 10–30.

[9] N. D. DUC, P. T. THANG, AND N. T. DAO ET AL., *Nonlinear buckling of higher deformable S-FGM thick circular cylindrical shells with metal–ceramic–metal layers surrounded on elastic foundations in thermal environment,* Compos. Struct., 121 (2015), pp. 134–141.

[10] N. D. DUC, AND P. T. THANG, *Nonlinear dynamic response and vibration of shear deformable imperfect eccentrically stiffened S-FGM circular cylindrical shells surrounded on elastic foundations,* Aerosp. Sci. Technol., 40 (2015), pp. 115–127.

[11] D. V. DUNG, AND L. K. HOA, *Nonlinear torsional buckling and postbuckling of eccentrically stiffened FGM cylindrical shells in thermal environment,* Compos. Part B, 69 (2015), pp. 378–388.

[12] M. SABZIKAR BOROUJERDY, R. NAJ, AND Y. KIANI, *Buckling of heated temperature dependent FGM cylindrical shell surrounded by elastic medium,* J. Theorey Appl. Mech., 2(4) (2014), pp. 869–881.

[13] F. TORNABENE, N. FANTUZZI, AND E. VIOLA, ET AL., *Winkler–Pasternak foundation effect on the static and dynamic analyses of laminated doubly-curved and degenerate shells and panels,* Compos. Part B, 57 (2014), pp. 269–296.

[14] N. D. DUC, AND T. Q. QUAN, *Transient responses of functionally graded double curved shallow shells with temperature-dependent material properties in thermal environment,* Euro. J. Mech. A Solids, 47 (2014), pp. 101–123.

[15] N. D. DUC, AND T. Q. QUAN, *Nonlinear thermal stability of eccentrically stiened FGM double curved shallow shells,* J. Thermal. Stress, 40(2) (2017), pp. 211–236.

[16] A. H. SOFIYEV, AND O. AKSOGAN, *Buckling of a conical thin shell with variable thickness under a dynamic loading,* J. Sound. Vib., 270 (2004), pp. 903–915.

[17] R. NAJ, M. SABZIKAR BOROUJERDY, AND M. R. ESLAMI, *Thermal and mechanical instability of functionally graded truncated conical shells,* Thin-Walled Struct., 46 (2008), pp. 65–78.

[18] A. H. SOFIYEV, *Non-linear buckling behavior of FGM truncated conical shells subjected to axial load,* Int. J. Non-Linear Mech., 46 (2011), pp. 711–719.

[19] D. V. DUNG, L. K. HOA, AND N. T. NGA, ET AL., *Instability of eccentrically stiffened func-*

tionally graded truncated conical shells under mechanical loads, Compos. Struct., 106 (2013), pp. 104–113.

[20] J. TORABI, Y. KIANI, AND M. R. ESLAMI, *Linear thermal buckling analysis of truncated hybrid FGM conical shells,* Compos. Part B, 50 (2013), pp. 265–272.

[21] N. D. DUC, AND P. H. CONG, *Nonlinear thermal stability of eccentrically stiffened functionally graded conical shells surrounded on elastic foundations,* Euro. J. Mech. A Solids, 50 (2015), pp. 120–131.

[22] J. E. JAM, AND Y. KIANI, *Buckling of pressurized functionally graded carbon nanotube reinforced conical shells,* Compos. Struct., 125 (2015), pp. 586–595.

[23] A. H. SOFIYEV, *Nonlinear free vibration of shear deformable orthotropic functionally graded cylindrical shells,* Compos. Struct., 142 (2016), pp. 35–44.

[24] D. V. DUNG, AND D. Q. CHAN, *Analytical investigation on mechanical buckling of FGM truncated conical shells reinforced by orthogonal stiffeners based on FSDT,* Compos. Struct., 159 (2017), pp. 827–841.

[25] N. D. DUC, K. S. EOCK, AND D. Q. CHAN, *Thermal buckling analysis of FGM sandwich truncated conical shells reinforced by FGM stiffeners resting on elastic foundations using FSDT,* J. Thermal Stress, 41(3) (2018), pp. 331–365.

[26] J. ZHANG, G. P. ZHAO, AND T. J. LU, *Dynamic Responses of Sandwich Beams with Gradient-Density Aluminum Foam Cores,* Int. J. Protec. Struct., 2(4) (2011), pp. 439–451.

[27] D. CHEN, J. YANG, AND S. KITIPORNCHAI, *Elastic Buckling and Static Bending of Shear Deformable Functionally Graded Porous Beam,* Compos. Struct., 133 (2015), pp. 54–61.

[28] D. CHEN, S. KITIPORNCHAI, AND J. YANG, *Nonlinear free vibration of shear deformable sandwich beam with a functionally graded porous core,* Thin-Walled Struct., 107 (2016), pp. 39–48.

[29] N. FOUDA, T. EL-MIDANY, AND A. M. SADOUN, *Bending, buckling and vibration of a functionally graded porous beam using finite elements,* J. Appl. Comput. Mech., 3(4) (2017), pp. 274–282.

[30] N. WATTANASAKULPONG, A. CHAIKITTIRATANA, AND S. PORNPEERAKEAT, *Chebyshev collocation approach for vibration analysis of functionally graded porous beams based on third-order shear deformation theory,* Acta. Mech. Sinica, 34(6) (2018), pp. 1124—1135.

[31] N. ZIANE, S. A. MEFTAH, AND G. RUTA ET AL., *Thermal effects on the instabilities of porous FGM box beams,* Eng. Struct., 134 (2017), pp. 150–158.

[32] M. BAMDAD, M. MOHAMMADIMEHR, AND K. ALAMBEIGI, *Analysis of sandwich Timoshenko porous beam with temperaturedependent material properties: Magneto-electro-elastic vibration and buckling solution,* J. Vib. Control, 25(23-24) (2017), pp. 2875–2893.

[33] G. L. SHE, F. G. YUAN, AND Y. REN, ET AL., *Nonlinear bending and vibration analysis of functionally graded porous tubes via a nonlocal strain gradient theory,* Compos. Struct., 203 (2018), pp. 614–623.

[34] G. L. SHE, F. G. YUAN, AND B. KARAMI, ET AL., *On nonlinear bending behavior of FG porous curved nanotubes,* Int. J. Eng. Sci., 135 (2019), pp. 58–74.

[35] M. JABBARI, M. REZAEI, AND A. MOJAHEDIN, ET AL., *Mechanical buckling of FG saturated porous rectangular plate under temperature field,* Iran J. Mech. Eng., 17(1:26) (2016), pp. 61–78.

[36] M. JABBARI, M. HASHEMITAHERI,AND A. MOJAHEDIN, ET AL., *Thermal buckling analysis of functionally graded thin circular plate made of saturated porous materials,* J. Thermal Stress, 2014; 37(2) (2014), pp. 202–220.

[37] A. R. KHORSHIDVAND, E. F. JOUBANEH, AND M. JABBARI, ET AL., BUCKLING ANALYSIS OF A POROUS CIRCULAR PLATE WITH PIEZOELECTRIC SENSOR–ACTUATOR LAYERS UNDER UNIFORM RADIAL COMPRESSION, Acta. Mech., 225(1) (2014), pp. 179—193.

[38] A. MOJAHEDIN, M. JABBARI,AND A. R. KHORSHIDVAND, ET AL., *Buckling analysis of func-*

tionally graded circular plates made of saturated porous materials based on higher order shear deformation theory, Thin-Walled Struct., 99 (2016), pp. 83—90.

[39] A. G. ARANI, M. KHANI AND Z. K. MARAGHI, *Dynamic analysis of a rectangular porous plate resting on an elastic foundation using high-order shear deformation theory,* J. Vib. Control, 24(16) (2018), pp. 3698–3713.

[40] F. EBRAHIMI, A. JAFARI, AND M. R. BARATI, *Vibration analysis of magneto-electro-elastic heterogeneous porous material plates resting on elastic foundations,* Thin-Walled Struct., 119 (2017), pp. 33—46.

[41] J. ZHAO, F. XIE, AND A. WANG, ET AL., *Vibration behavior of the functionally graded porous (FGP) doubly-curved panels and shells of revolution by using a semi-analytical method,* Compos. Part B, 157 (2019), pp. 219–238.

[42] N. D. DUC, V. D. QUANG, AND P. D. NGUYEN, ET AL., *Nonlinear dynamic response of functionally graded porous plates on elastic foundation subjected to thermal and mechanical loads,* J. Appl. Comput. Mech., 4(4) (2018), pp. 245–259.

[43] Y. Q. WANG, *Electro-mechanical vibration analysis of functionally graded piezoelectric porous plates in the translation,* Acta. Astro., 143 (2018), pp. 263–271.

[44] S. COSKUN, J. KIM, AND H. TOUTANJI, *Bending, Free vibration, and buckling analysis of functionally graded porous micro-plates using a general third-order plate theory,* J. Compos. Sci., 3(1) (2019), 15, https://doi.org/10.3390/jcs3010015.

[45] Y. XUE, G. JIN, AND X. MA, ET AL., *Free vibration analysis of porous plates with porosity distributions in the thickness and in-plane directions using isogeometric approach,* Int. J. Mech. Sci., 152 (2019), pp. 346–362.

[46] V. H. NAM, N. T. PHUONG, D. T. DONG, N. T. TRUNG, AND N. V. TUE, *Nonlinear thermomechanical buckling of higher-order shear deformable porous functionally graded material plates reinforced by orthogonal and/or oblique stiffeners,* Proc IMechE, Part C: J. Mech. Eng. Sci., 223(17) (2019), pp. 6177–6196.

[47] Y. WANG, AND D. WU, *Free vibration of functionally graded porous cylindrical shell using a sinusoidal shear deformation theory,* Aerosp. Sci. Technol., 66 (2017), pp. 83–91.

[48] H. LI, F. PANG, AND H. CHEN, ET AL., *Vibration analysis of functionally graded porous cylindrical shell with arbitrary boundary restraints by using a semi analytical method,* Compos. Part B Eng., 164 (2019), pp. 249–264.

[49] V. H. NAM, N. T. TRUNG, AND L. K. HOA, *Buckling and postbuckling of porous cylindrical shells with functionally graded composite coating under torsion in thermal environment,* Thin-Walled Struct., 144 (2019), 106253, https://doi.org/10.1016/j.tws.2019.106253.

[50] H. LI, F. PANG, AND Y. REN, ET AL., *Free vibration characteristics of functionally graded porous spherical shell with general boundary conditions by using frst-order shear deformation theory,* Thin-Walled Struct., 144 (2019), 106331, https://doi.org/10.1016/j.tws.2019.106331.

[51] M. RAHMANI, Y. MOHAMMADI, AND F. KAKAVAND, *Vibration analysis of sandwich truncated conical shells with porous FG face sheets in various thermal surroundings,* Steel Compos. Struct., 32(2) (2019), pp. 239–252.

[52] D. K. THAI, T. M. TU, AND L. K. HOA, ET AL., *Nonlinear stability analysis of eccentrically stiffened functionally graded truncated conical sandwich shells with porosity,* Materials, 6 (2018), pp. 11(11). pii: E2200. doi: 10.3390/ma11112200.

[53] M. BARUCH, O. HARARI, AND J. SINGER, *Low buckling loads of axially compressed conical shells,* J. Appl. Mech., 37 (1970), pp. 384–392.

[54] C. S. XU, Z. Q. XIA, AND C. Y. CHIA, *Nonlinear theory and vibration analysis of laminated truncated thick conical shells,* Int. J. Non-Linear Mech., 31(2) (1996), pp. 39–54.

[55] L. TONG, AND T. K. WANG, *Simple solutions for buckling of laminated conical shells,* Int. J. Non-Linear Mech., 34(2) (1992), pp. 93–111.
[56] D. O. BRUSH, AND B. O. ALMORTH, Buckling of Bars, Plates and Shells, New York: McGraw-Hill, 1975.
[57] A. S. VOLMIR, The Stability of Deformable Systems, Moscow: Nauka, 1967.